AN EUV IMAGING SPECTROGRAPH FOR HIGH-RESOLUTION OBSERVATIONS OF THE SOLAR CORONA

WERNER M. NEUPERT, GABRIEL L. EPSTEIN*, ROGER J. THOMAS

Laboratory for Astronomy and Solar Physics, NASA / Goddard Space Flight Center, Greenbelt, MD 20771, U.S.A.

and

WILLIAM T. THOMPSON

Applied Research Corporation, Landover, MD 20785, U.S.A.

(Received 17 May, 1991)

Abstract. An extreme ultraviolet (EUV) imaging spectrograph for the wavelength range from 235 to 450 Å has been developed and used for high resolution observations of the Sun. The instrument incorporates a glancing incidence Wolter Type II Telescope and a near-normal incidence toroidal grating spectrograph to achieve near-stigmatic performance over this spectral range. The design of the spectrograph entrance aperture enables both stigmatic spectra with spectral resolution adequate to observe emission line profiles and spectroheliograms of restricted portions of the Sun to be obtained concurrently. In this paper we describe the design and performance of the instrument and provide an overview of results obtained during a sounding rocket flight on May 5, 1989.

1. Introduction

Observation of coronal emission lines has long been recognized as an important means of investigating the dynamic properties of coronal plasmas and addressing fundamental questions regarding coronal heating, solar wind acceleration and the origin of flares (Athay, 1976). Nonetheless, observations adequate in both spectral and spatial resolution to provide quantitative information on emission line profiles on small spatial scales continue to be an experimental challenge. Although spectroscopic observations of the low corona above the solar limb can be made with ground-based coronagraphs (Billings, 1966), uncertainties due to the possible integration over many emission sources along a line of sight and the lack of correlative observations of the underlying photosphere and chromosphere limit their usefulness. By observing the emission line corona at extreme ultraviolet (EUV) wavelengths, one immediately has access to the lower corona over the visible disk of the Sun in a multitude of lines that encompass a wide range of electron temperatures, provide spectral diagnostics for electron densities, and can be used to probe the dynamic properties of the coronal plasma.

We have designed and developed an instrument operating at EUV wavelengths that can obtain measurements of coronal emission line profiles adequate to study the physical state of the coronal plasma, with spatial resolution sufficient to identify the type

* Present address: X-ray Timing Explorer Project Code 410, NASA/Goddard Space Flight Center, Greenbelt, MD 20771, U.S.A.

Solar Physics **137:** 87–104, 1992.

of coronal structure or feature in which the emission originates and its underlying photospheric and chromospheric counterparts. The unique design of the instrument enables acquisition of both high-resolution spectra and monochromatic images of a region in rapid sequence and hence is well-suited for a short duration rocket flight. The resulting instrument, called SERTS (for Solar EUV Rocket Telescope and Spectrograph) is an imaging EUV spectrograph capable of providing nearly stigmatic performance over a spectroscopically important range of wavelengths from 235 to 450 Å. It was initially proposed to NASA as a payload for the Space Shuttle (Neupert *et al.*, 1978, 1981). This paper discusses its design, as modified for use on a sounding rocket, and presents results of a rocket flight on May 5, 1989 that demonstrate characteristics of its performance.

2. Concept of the Instrumentation

The objective of the program was an instrument that could retain the stigmatic imaging capability of the NRL Spectroheliograph (SO 82A) on Skylab (Tousey *et al.*, 1977) while providing greater spatial selectivity so that image overlap in spectral regions with numerous emission lines would be reduced. Another equally important objective was the capability to achieve high spectral resolution but with lesser spatial convolution than has been present in earlier instruments flown to observe the EUV corona (Feldman and Behring, 1974; Cushman and Rense, 1978; Rottman, Orrall, and Klimchuk, 1981). The present design achieves these objectives by introducing an imaging fore-optic with its image plane at the entrance aperture of a toroidal grating spectrograph so that either spectra or spectroheliograms with high spatial selectivity can be obtained, depending on the configuration of the entrance aperture.

The incoming radiation is imaged on the entrance aperture of the spectrograph by a Wolter Type II telescope (Mangus, 1970). Sensitivity over a broad spectral band was an important initial consideration, in order to use widely spaced pairs of lines for temperature and density measurements, and the grazing incidence design of the telescope provides adequate EUV reflectivity over the wavelength range of the spectrograph for this purpose. The spectrograph is used at near-normal incidence and provides stigmatic imaging at two wavelengths and acceptable imaging over the entire range. The resulting images are recorded on Eastman Kodak 101–07 EUV-sensitive photographic film that is advanced frame-by-frame during the rocket flight with a suitable transport mechanism. The front face of the entrance aperture is polished so that light from portions of the solar image not admitted to the spectrograph is reflected to a slit jaw camera capable of recording sunspots and the solar limb. The optical layout of the instrument is shown in Figure 1. The following sections provide details of the design of the instrument.

3. Telescope Design

Design characteristics of the Wolter Type II telescope, which has a parabolic primary and hyperbolic secondary, are provided in Table I. A full figure of revolution rather than

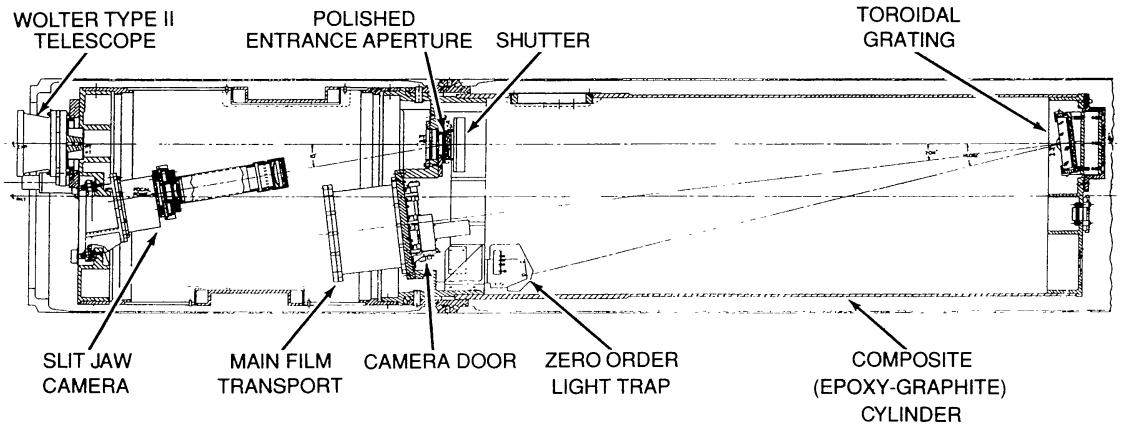

Fig. 1. Plan of the EUV imaging spectrograph SERTS (Solar EUV Rocket Telescope and Spectrograph) showing location of optical elements and film cameras. The instrument is designed as two major mechanical sections cantilevered from a central bulkhead. The spectrograph section is a carbon composite material for thermal stability.

a sector design was chosen for this optical element because of the greater ease of fabrication, assembly and alignment afforded by the symmetry of the design. Glancing angles of incidence between 10° and 13° are used to optimize reflectivity and aperture in the 200–450 Å range. The resulting aperture area is nearly half (47%) of that available with an unobscured aperture. Alignment tolerances between optical elements of the Type II design are stringent because of the magnification introduced by the Cassegrain

TABLE I

Wolter Type II telescope design parameters

Effective focal length	212 cm
Maximum slope angle	13°
Minimum slope angle	9.45°
Overall length (to focus)	79.3 cm
f/No.	*f*/22
Nominal geometric aperture area	35 cm^2
Nominal RMS surface accuracy: paraboloid	109 nm
hyperboloid	97 nm
Measured resolution (laboratory) at 304 Å	6 arc sec
Nominal reflectivity (per surface) at 10° glancing angle	0.57 at 250 Å to 0.63 at 450 Å

design (nominal optical tolerances scale inversely with the square of the magnification of the system, which is 19 for this particular design). The OPSTOP ray tracing program was used to establish alignment tolerances between the two elements: to focus 80% of the rays in a 15 micron diameter (1.5 arc sec) spot requires an alignment tolerance of ± 0.36 μ in decenter and 2.1 arc sec in tilt. Actual alignment between paraboloid and hyperboloid was 0.68 μ in decenter and 0.8 arc sec in tilt. In practice, image quality was limited by the quality of the optical surfaces. Early laboratory tests demonstrated that the assembled telescope could resolve two imaged slits separated by 3 arc sec at 5461 Å and two slits separated by 6 arc sec at 304 Å. Later tests at 304 Å showed that image

contrast (but not limiting resolution) could be improved by masking the inner portion of the annular aperture, and that was the configuration flown in 1989. (A new telescope with significantly better performance has subsequently been built and will be used on the next SERTS flight.) The spatial modulation transfer function of the assembled instrument was derived from the image of a small emission source at 304 Å recorded near the location of best focus during the rocket flight and implied a spatial resolution of 7 arc sec for this high-contrast source. Spatial resolution of the SERTS in the direction of dispersion is ultimately limited to 2–3 arc sec by the widths of the spectral lines.

All optical components of the telescope assembly were fabricated of Cer-Vit, a ceramic material supplied by the Owens-Illinois Glass Co., to minimize figure deterioration due to stress in a changing thermal environment. An epoxy with good thermal conductivity, EPON 815/TETA, thinned 50% by weight with methyl ethyl ketone, was used to bond the components. The telescope was originally designed, assembled, and tested as a prototype for a potential Solar Maximum Mission instrument by the Space Systems Department, Valley Forge Space Center of the General Electric Co. Optical components of the telescope were fabricated by the Optics Branch of the Goddard Space Flight Center.

A disadvantage of the telescope design is the appreciable curvature of its focal plane, resulting in a variation of spatial resolution over the field of view of the instrument. It was decided that best spatial focus should be located within the large apertures (see next section) where spectroheliograms would be obtained. This was accomplished by locating the planar entrance aperture of the spectrograph inside the axial focus location of the EUV focus (by 5.5 mm for the telescope used in the 1989 flight), so that the focal curve of the telescope, as measured in the laboratory, intersected the entrance aperture plane of the spectrograph at approximately 5 arc min from its on-axis line of sight.

4. Spectrograph Design

The use of a toroidal grating to achieve stigmatic imaging was originally pointed out by Haber (1950) and has more recently been discussed by Samson (1967), Feldman *et al.* (1976), and Huber and Tondello (1979). The present design has been optimized for the 235 Å to 450 Å spectral range using a mechanically ruled tripartite grating with 3600 grooves mm^{-1} produced by Hyperfine, Inc. Grating parameters and design characteristics of the spectrograph are given in Table II. Evaluation of grating reflectivity at EUV wavelengths is discussed by Thomas *et al.* (1991). The short wavelength limit was based on a desire to include a density-sensitive couplet of Fe IX emission lines at 242 Å and 245 Å (Feldman, Doschek, and Widing, 1978; Haug, 1979), recognizing that the rapid decrease in grating reflectivity below 300 Å would make long exposures necessary for these lines (which would not have been a problem in a long-duration Space Shuttle mission). The upper limit was dictated by mechanical design limitations of the camera system and the desire to maximize the dispersion of the instrument for emission line profile studies. The optical design provides stigmatic imaging at 286 Å and 392 Å

TABLE II

SERTS toroidal grating spectrograph parameters

Ruling density:	
primary rulings	3600 grooves mm^{-1}
focus rulings	342 grooves mm^{-1}
Radii of curvature:	
sagittal	1200.02 mm
tangential	1209.67 mm
Measured surface accuracy	better than 0.08 wave peak to peak at 6328 Å
Blaze angle	2.8°
Spectral range	235–450 Å
Radius of cylindrical focal plane	647.2 mm
Nominal stigmatic wavelengths	285.9 Å and 392.1 Å
Dispersion at focal plane	2.2 Å mm^{-1}

(Figure 2). The spectrograph has been optimized for spectral resolution by locating the cylindrical film plane on the tangential focus of the grating. The optimum radius of this film plane was determined by minimizing computed spot sizes on a cylindrical surface. Spectral resolution is nominally best in the plane of the grating normal, with an computed image width of less than 5 μ (11 mÅ) for a point source on the entrance

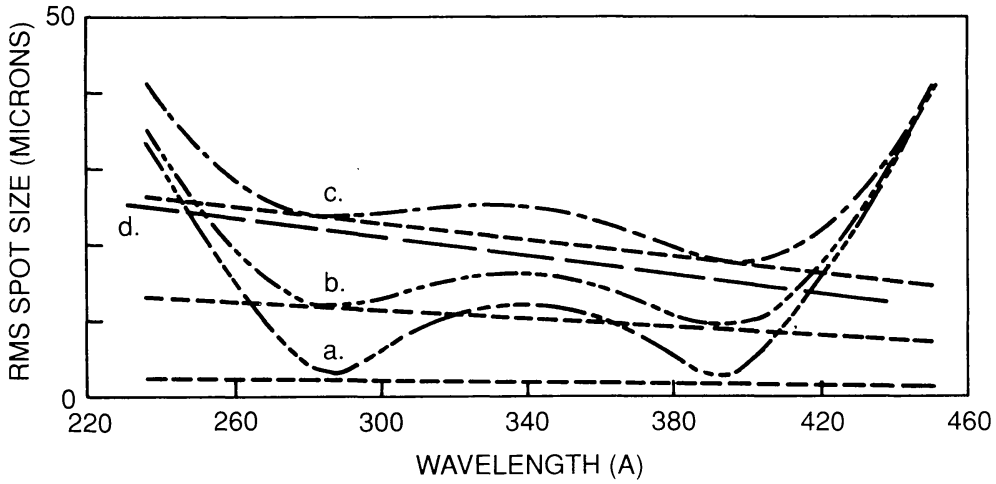

Fig. 2. Calculated spectral (dashed lines) and spatial (dot-dashed lines) resolution vs wavelength for the SERTS spectrograph. The plotted curves are calculated RMS spot heights and widths for point sources at three different locations on the entrance aperture: (a) on the Rowland plane and (b) and (c) at off-plane positions corresponding to angular deviations of 5 and 10 arc min in the instrument's field of view. Also shown, as a heavy dashed line (d), is the effective instrumental width obtained at the center of the entrance aperture during flight on May 5, 1989.

aperture. Spectral blur increases with increasing off-plane locations and must be taken into account when analyzing spectral line widths. Off-plane spectral resolution improves slightly with increasing wavelength. Typical spot diagrams for a monochromatic point source on the entrance aperture are illustrated in Figure 3 for two spectral locations, one

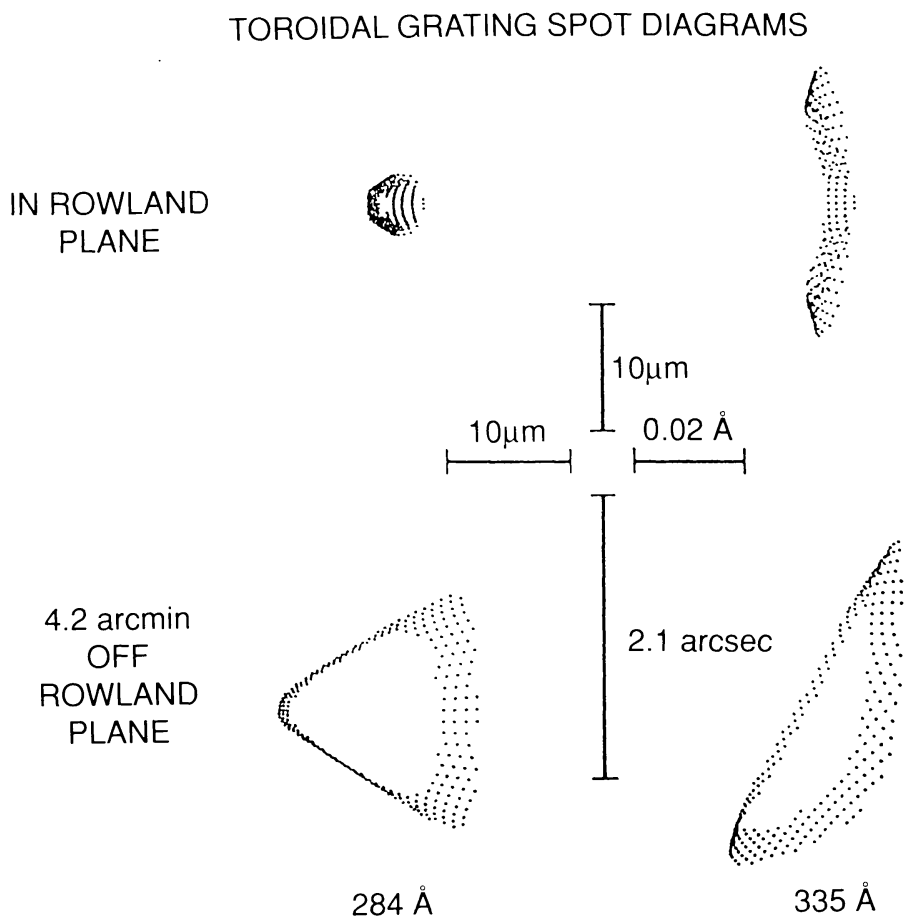

Fig. 3. Spot diagrams of rays intersecting the SERTS spectrograph focal plane for two wavelengths (one at a stigmatic focus, the other midway between the two stigmatic foci) and at two vertical locations in the film plane.

at a stigmatic wavelength and the other midway between the two stigmatic wavelengths. Spatial resolution is improved over the 0.3×0.9 arc min resolution achieved by Rottman, Orrall, and Klimchuk (1981) or the 20 arc sec resolution of an earlier instrument flown by Cushman and Rense (1978), both of which measured coronal velocities using Doppler shifted emission lines. The f/number of extreme rays in the present optical system is $f/22$. A slower system would have provided improved resolution but at the expense of system through pout.

To maximize the recorded emission line profiles relative to the grain of the photographic emulsion, the spectrograph was used in a magnifying configuration with $m = 1.100$. Ray tracing demonstrated that this had a negligible effect on image quality. Spatial resolution of the spectrograph, also shown in Figure 2, was a secondary consideration, given the limited performance of the existing telescope, the fact that resolution would be further compromised by the curved focal plane of the telescope, and the unavoidable blurring in the direction of dispersion due to finite spectral line widths.

4.1. Spectrograph Data Format

The SERTS design uses a unique spectrograph entrance aperture configuration that enables two types of observations concurrently: (a) stigmatic imaging with high spectral resolution along a chord in the field of view, using a narrow entrance slit centered on the optic axis of the telescope and on the Rowland plane of the spectrograph; and (b) stigmatic imaging with spatial coverage, accomplished by opening up the off-plane portions of the entrance slit to produce a wider field of view in the dispersion direction. This entails a compromise between the amount of solar area covered and the acceptable amount of overlap of images of adjacent spectral lines. The geometry of the entrance aperture is shown in Figure 4, which is labeled with the corresponding angular dimensions of the field of view when used with the current telescope. The resultant data record is a re-imaging of the compound aperture in each spectral line. The degree of solar image overlap for adjacent spectral lines in the upper and lower panels is only about one-sixth

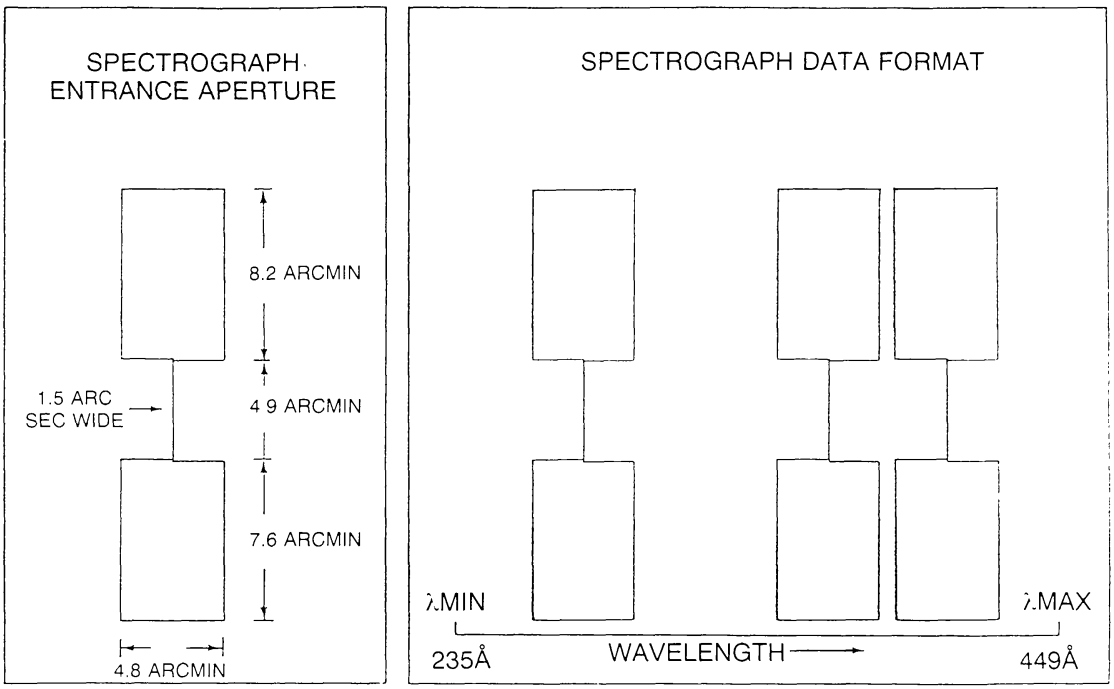

Fig. 4. Format of data in the focal plane of the SERTS toroidal grating spectrograph. Each spatial element of the entrance aperture is re-imaged in the focal plane at each incident wavelength. The narrow central portion provides high spectral resolution while the upper and lower panels provide spectroheliograms.

of that encountered in the slitless Wadsworth spectrograph design employed by the NRL SO 82A instrument on Skylab (Tousey *et al.*, 1977). Consequently, distributed sources on the solar disk can be studied with far less spatial and spectral ambiguity than with the earlier design. The overall extent of the entrance aperture covers 21 arc min on the solar disk, matching the usable width of 35 mm photographic emulsion and available film transport mechanisms. A nominal slit width of 16 μ, corresponding to a instrumental line width of 39 mÅ, was used for the spectral portion of the observations.

The polished front surface of the spectrograph aperture plate is tilted 5 deg from being normal to the telescope's optical axis so that the solar image surrounding the entrance aperture is directed to an auxiliary film camera. A broad-band filter (3835 ± 30 Å) provides images of sunspots and the solar limb with good contrast. Images were recorded on Eastman Kodak 649 emulsion at 11 s intervals during the flight and used to confirm the pointing direction of the optical axis of the instrument for each primary observation. A 1500 Å thick filter of aluminium-silicon (99%/1%) was used for rejection of the visible and near UV spectrum in the spectrograph. This filter was mounted directly behind the entrance aperture.

4.2. Spectrograph assembly and alignment

The instrument was mechanically designed with two sections cantilevered from a central bulkhead (Figure 1). The forward section carries the telescope on the exterior of the forward bulkhead and a slit jaw camera system, viewing the spectrograph entrance aperture, on the inner side of that bulkhead. The rear section carries the grating mount and pump-out apertures, which are electrostatically screened (+ and − 28 V) to minimize the migration of charged particles into the vicinity of the photographic film. The spectrograph entrance aperture, a trap for zero-order radiation, and the main film camera are mounted on the central bulkhead. Provision is made for a shutter directly behind the entrance aperture. A carbon composite is used for the spectrograph (rear) section to minimize image defocus due to temperature increases during the ascent of the rocket. Thirty-two separate isolation pads of Vespel SP21 (a polyamide resin with 15% graphite) are located in a ring between the outer housing of the payload and the central bulkhead to minimize conduction of heat to the instrument during ascent of the rocket.

To facilitate initial alignment and testing, a set of low-density rulings, at 342 grooves mm^{-1}, was placed on both sides of the prime ruling. These coarse rulings shifted the operating wavelength range (and stigmatic wavelengths) of the spectrograph into the near UV, so that the initial optical setup could be carried out in air with a mercury emission line source. Focus was located by taking a series of exposures with the film camera moved in small increments through the predicted location of the spectral focus. The separations of the out-of-focus images of the two side panels were then used to determine the location of best spectral focus. The same procedure was repeated at EUV wavelengths using a D.C. gas discharge source with a helium/neon gas mixture and illuminating only the extreme sides of the high-density portion of the grating. The final film plane was within 90 μ of best focus over the measured range of 304 to 446 Å. This displacement corresponds to a blur circle of 3 μ, which is negligible compared to optical aberrations and photographic film granularity. A final focus assessment was carried out with an annular grating mask approximating the pattern of illumination that would be encountered in actual solar observations with the Wolter telescope in place.

4.3 Calibration and in-flight performance

A relative calibration of the instrument over its operation range has been obtained by two methods. The solar spectrum itself provides a means for obtaining such a calibra-

tion, using spectral line ratios that are insensitive to variations in coronal temperature and density (Neupert and Kastner, 1983). Results from this method are given in Figure 5. We have assumed that the sensitivity of the photographic emulsion (defined as photographic density per unit incident energy) is constant throughout the range of wavelengths covered by SERTS, based on previous measurements by Burton, Hatter, and Ridgeley (1973) at wavelengths from 735 Å to 1800 Å.

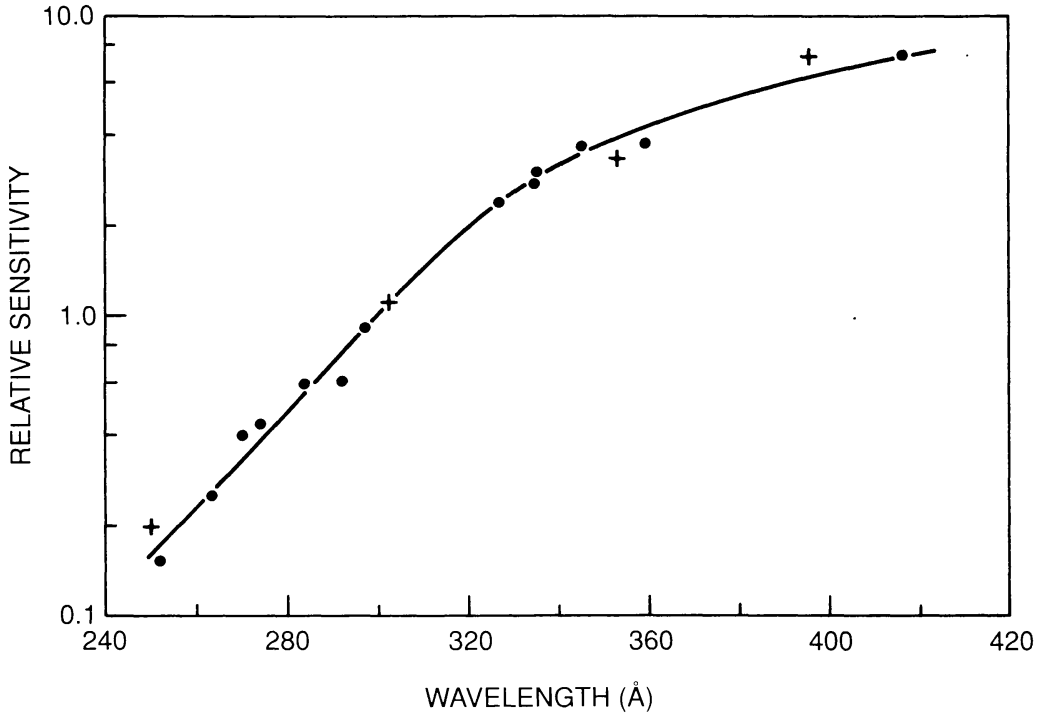

Fig. 5. Relative efficiency of the SERTS optical system derived from emission line ratios that are independent of the density and temperature of the emitting plasma (Neupert and Kastner, 1983). The resulting curve is normalized to 1.0 at 300 Å. For comparison, a calibration derived from measured and nominal reflectivities of the optical components and transmission of the aluminium blocking filter and scaled to match the spectroscopically derived curve is indicated by crosses at several wavelengths.

A calibration has also been achieved by combining measurements of individual components in the optical train. The reflectivity of the grating was measured using the SURF II facility at the National Institute of Standards and Technology (NIST) (Thomas *et al.*, 1991). For that measurement, the grating was set up in a Wadsworth mount configuration and the diffracted synchrotron radiation measured as function of wavelength with a previously calibrated anodized evaporated aluminium photodiode (Canfield, Johnston, and Madden, 1973). Grating reflectivity was then obtained by comparing the detected flux with the calculated flux incident on the grating from the synchrotron. Previous measurements (Osantowski, 1974) on the reflectivity of Cer-Vit in this spectral range were adopted for the telescope. Combining the results of measured and nominal values for the SERTS components produces a relative calibration consistent with the spectroscopic method. Figure 5 includes several values determined in

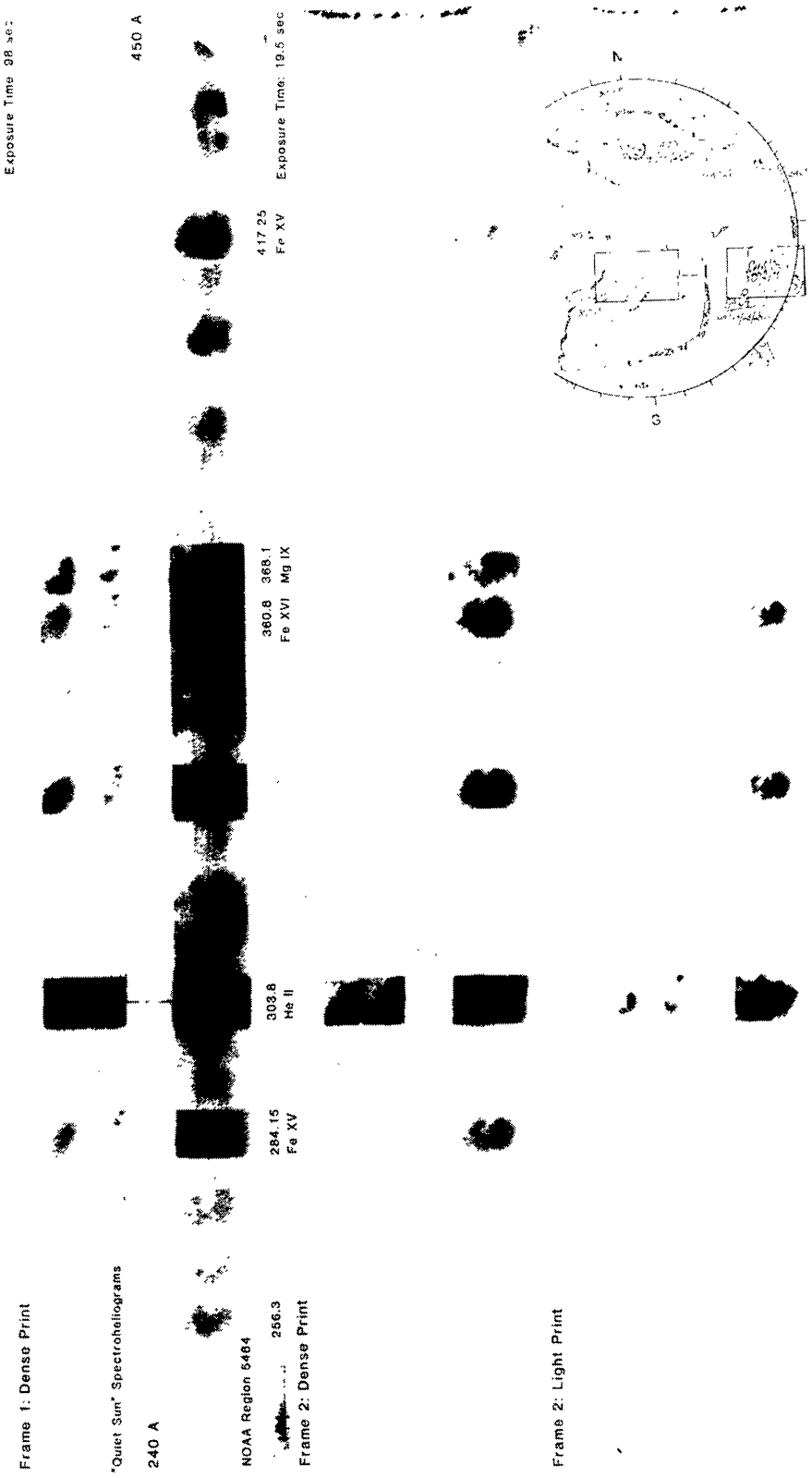

Fig. 6a. Stigmatic EUV spectra and spectroheliograms recorded on Kodak 101–07 emulsion by SERTS on May 5, 1989. Spectroheliograms of NOAA region 5464 were obtained in these exposures by centering one of the two large entrance apertures on the region. Data frame 2 is presented in both a dense and a light photographic print to show details in the spectroheliograms. Projection of the entrance aperture on the Sun is shown for each observation. Drawings of photospheric neutral lines, courtesy of David Speich, NOAA.

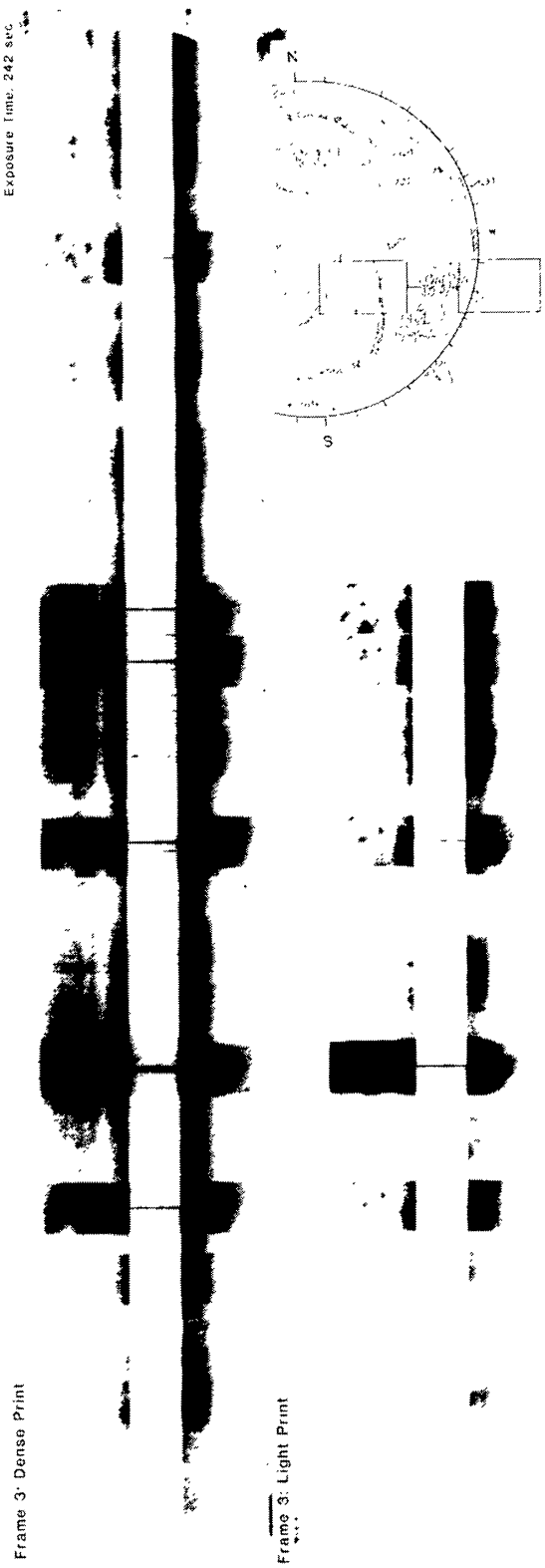

Fig. 6b. The optical axis of the instrument was repointed part-way through the rocket flight to center the narrow silt on the active region and thereby obtain high resolution near-stigmatic spectra of the large active region. As in Figure 6(a), both a dense and a light print of the single exposure are shown. Note the small compact sources of coronal emission present in areas with no evident photospheric activity.

this manner, normalized to the spectroscopically derived curve at 300 Å. The absolute sensitivity of the instrument can be estimated by normalizing the signal recorded in the strong He II line at 304 Å from the 'quiet' Sun to previously measured fluxes. Work is currently in progress in measuring the sensitivity of the photographic emulsion, again using the SURF II facility, and will be used to update our instrument calibrations.

Spectral resolution in the central portion of the entrance slit for the flight of May 5, 1989 is indicated in Figure 2 for a slit of zero width. Actual instrumental line widths for the flight data varied along the spectrograph slit, from 50 to 75 mÅ at 304 Å and from 45 to 60 mÅ at 420 Å. The location of best spectral resolution at final focus was offset vertically from the center of the entrance aperture images by approximately 3.7 mm, being located in one of the two larger entrance apertures. Notwithstanding this anomaly, probably due to a residual distortion of the grating in its mount, the resultant spectral resolution is comparable to or less than the thermal widths of emission lines of heavy ions such as Fe and is adequate to assess the contributions of non-thermal broadening in the observed spectral widths. In addition, the signal level of the major coronal lines was very high so that the centers of spectral line segments could be located to about 1 μ on the photographic record, providing a sensitivity to line-of-sight velocities of 2–3 km s^{-1} for these lines.

5. Flight Results

The instrument was flown on a Terrier-boosted Black Brant rocket on May 5, 1989 The target region for acquisition of both spectroheliograms and spectra was NOAA Region 5464, a large, stable active region with a beta-gamma-delta magnetic field characteristic. At the time of the flight its largest spot was located at S 18 W 45. To acquire spectroheliograms and stigmatic spectra of the same solar region it was merely necessary to make one change in pointing direction during the flight, with an angular displacement of the line of sight of about 5 arc min along the long dimension of the central slit. This was done about halfway through the observing sequence. The resulting images, together with a projection of the SERTS entrance slit on the Sun for each of the two pointing directions, are shown in Figures 6(a) and 6(b). One of the large entrance apertures was centered on the active region in Figure 6(a) and the narrow central slit was positioned on the region in Figure 6(b). These images represent the first recording of high-resolution EUV spectra essentially concurrent with spectroheliograms of the same region of the solar atmosphere. Using the auxiliary slit jaw camera data, we verified that images of two sunspots, including the largest one in the region, fell on the central portion of the narrow slit aperture while spectral observations of the active region were being taken. These features provided the means for spatially matching the flight data with ground-based observations to an estimated accuracy of 10 arc sec or better. The initial phase of a small flare was in progress at the time of the observations and a portion of it was observed along the narrow entrance slit. As a result, we obtained a stigmatic spectrum of EUV flare emission in addition to spectra and spectroheliograms of numerous other coronal features in the field of view.

Sequences of exposures with durations increasing by factors of five were planned. Because of a failure in the main camera control electronics part-way through the observing sequence, only two of three planned exposures were obtained at the first pointing location and a single long exposure, rather than the three planned exposures of 195, 39, and 8 s duration, was recorded at the second. As a result, the emission line and images of He II at 304 Å from the active region are severely overexposed.

5.1. Spectroheliograms

The resulting spectroheliograms demonstrate the capability of the instrument to provide non-overlapping spectroheliograms for the most intense emission lines if the proper exposure is selected. Spectroheliograms in the bright emission lines of Mg IX (368.1 Å) and Fe XVI (335.4 Å) together with ground-based observations of Hα and Ca II K are shown in Figure 7. In addition to spectroheliograms of the major active region, we recorded spectroheliograms of EUV emission over extensive portions of the Sun near the central meridian in which no activity other than several small bipolar regions was reported (Figure 6(b)). A study is under way to characterize the emissions of these minor regions in several strong EUV lines and to compare the results with known properties of X-ray bright points.

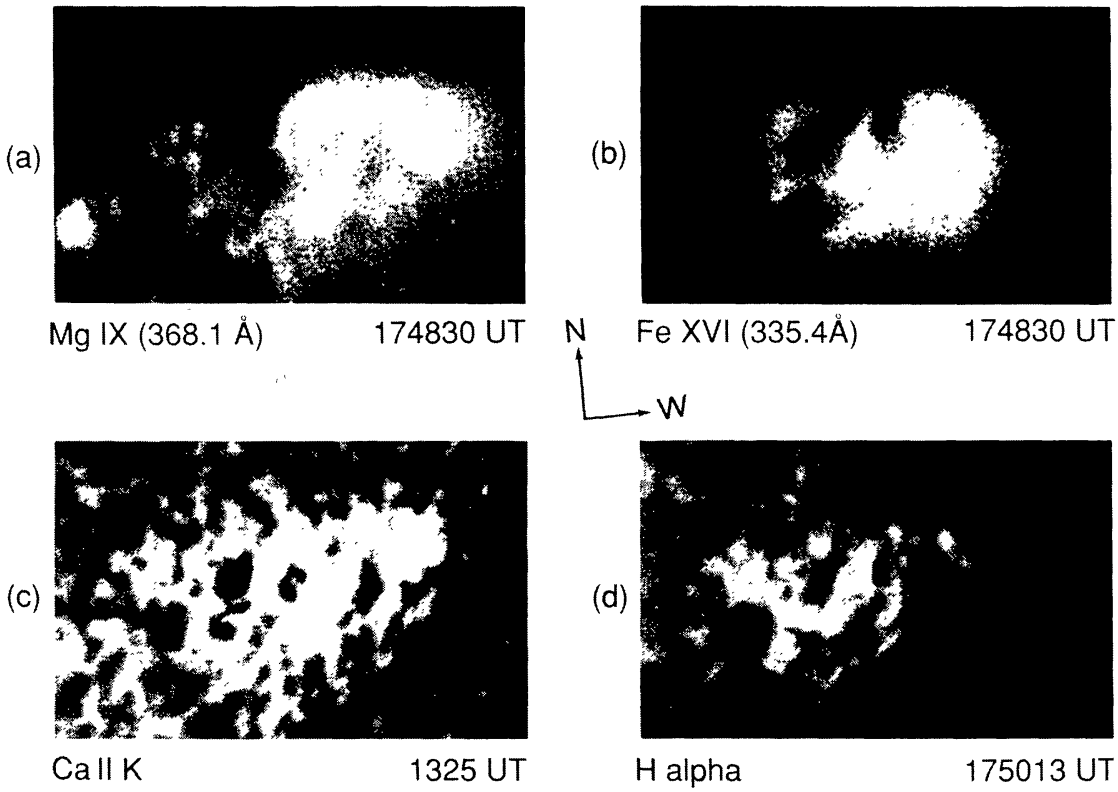

Fig. 7. Reproduction of EUV spectroheliograms of NOAA region 5464 in EUV emission lines of Mg IX and Fe XVI acquired at the pointing location shown in Figure 6(a) and compared with ground-based observations in Hα and in Ca II K. In this figure the images have been rotated counterclockwise by 90° relative to their orientation in Figure 6(a). Ca II K-spectroheliogram courtesy of Sacramento Peak Observatory, National Solar Observatory of the National Optical Astronomy Observatories. Hα filtergram courtesy of Big Bear Solar Observatory.

5.2. STIGMATIC SPECTRA

An enlarged portion of the exposure (shown its entirety in Figure 6(b)) taken with the 5 arc min long slit on the active region is illustrated in Figure 8 and demonstrates the stigmatic property of the instrument combined with high spectral resolution. In this spectrum the field of view in the direction of dispersion is nominally only 1.5 arc sec,

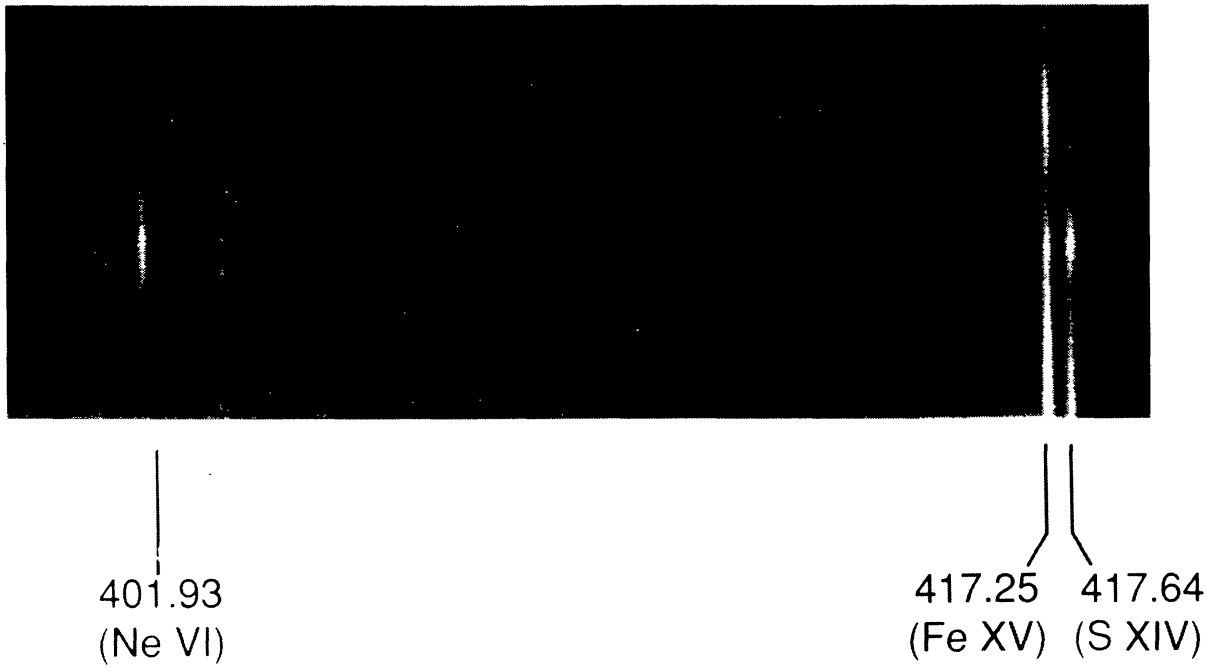

Fig. 8. Reproduction of a portion of the stigmatic EUV spectrum of NOAA region 5464 in the spectral range from 400 to 420 Å. Prominent spectral lines of Ne VI (401.93 Å), Fe XV (417.25 Å), and S XIV (417.64 Å) demonstrate the changing distribution of emission with temperature across the region.

but is degraded to about 7 arc sec by the limited resolution of the fore-optic and its curved image plane. Spatial resolution along the slit is comparable, for the same reasons. Comparison of the emission lines of Ne VI, Fe XV, and S XIV, formed at 0.45×10^6 K, 2.3×10^6 K, and 3.0×10^6 K, respectively, reveals marked changes in the spatial distribution of radiation with formation temperature of the emitting ion.

Figure 9(a–c) shows the distributions of emission across the active region for these and additional ions, encompassing among them a wide range of electron temperatures. Relatively small changes in electron temperature, as in progressing from one stage of ionization of iron to the next, result in significantly different distributions. These data are the first stigmatic spectral records to be obtained in the 200–400 Å range over a wide temperature range and demonstrate the dramatic variation in emission that can occur with even small changes in electron temperature in the corona over an active region.

The most intense emission source at the highest and lowest temperatures is associated with the pre-impulsive phase of the small flare, whose initial Hα enhancement can be detected on the centerline of the spectroheliogram of Figure 7. A striking observational result is the lack of flare-associated emission at intermediate coronal temperatures ($1.5–2.0 \times 10^6$ K), represented in Figure 9(b) by the Fe XIV ion. This suggests that the

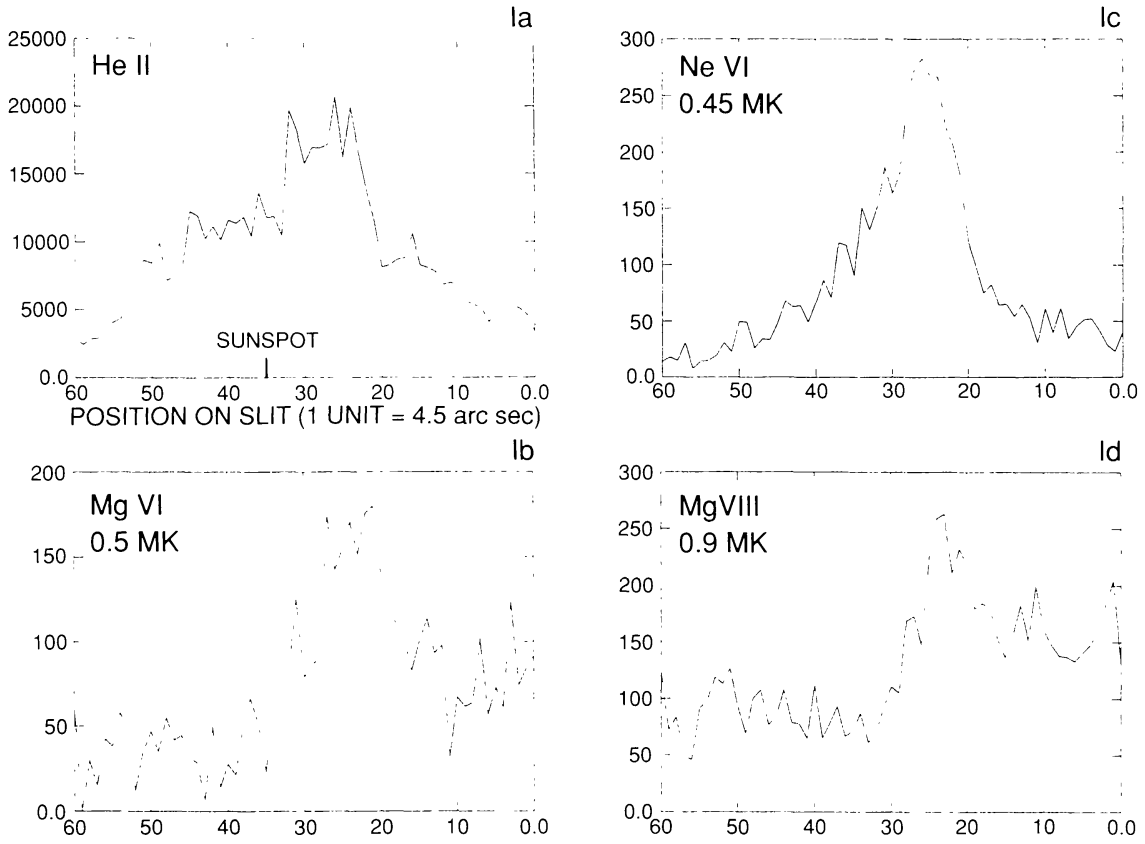

Fig. 9a.

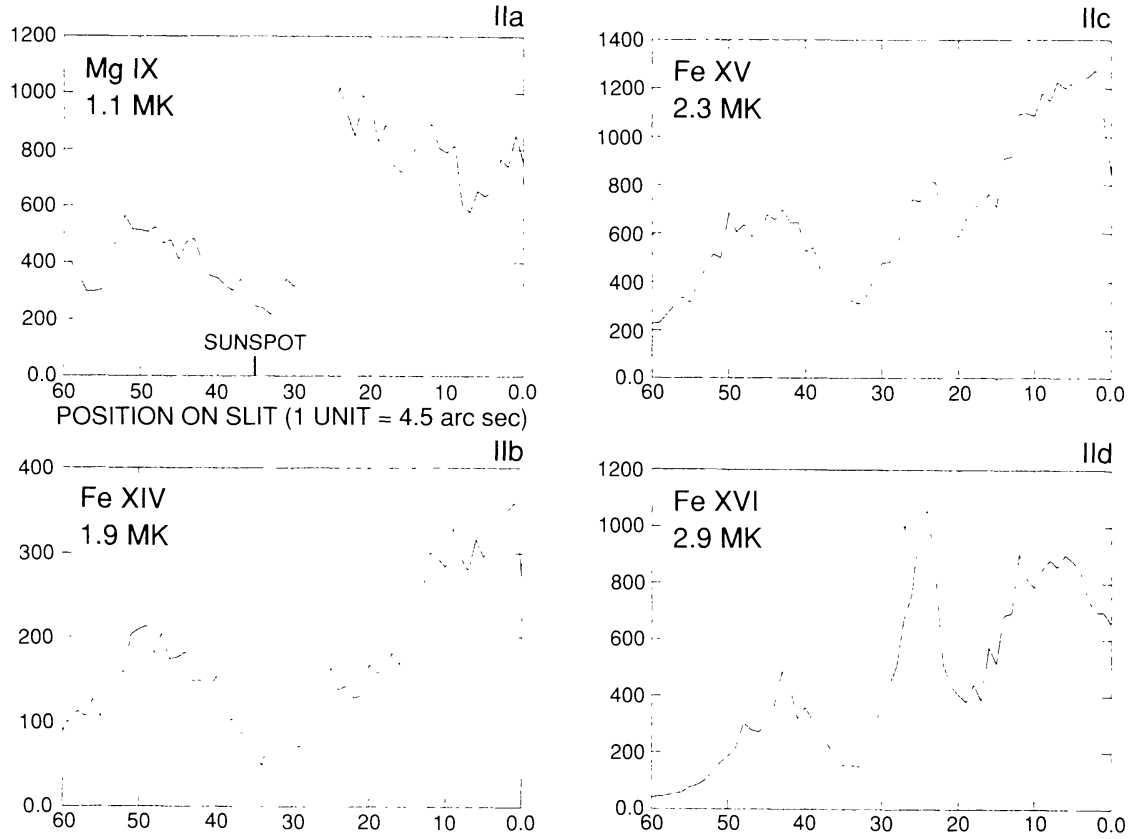

Fig. 9b.

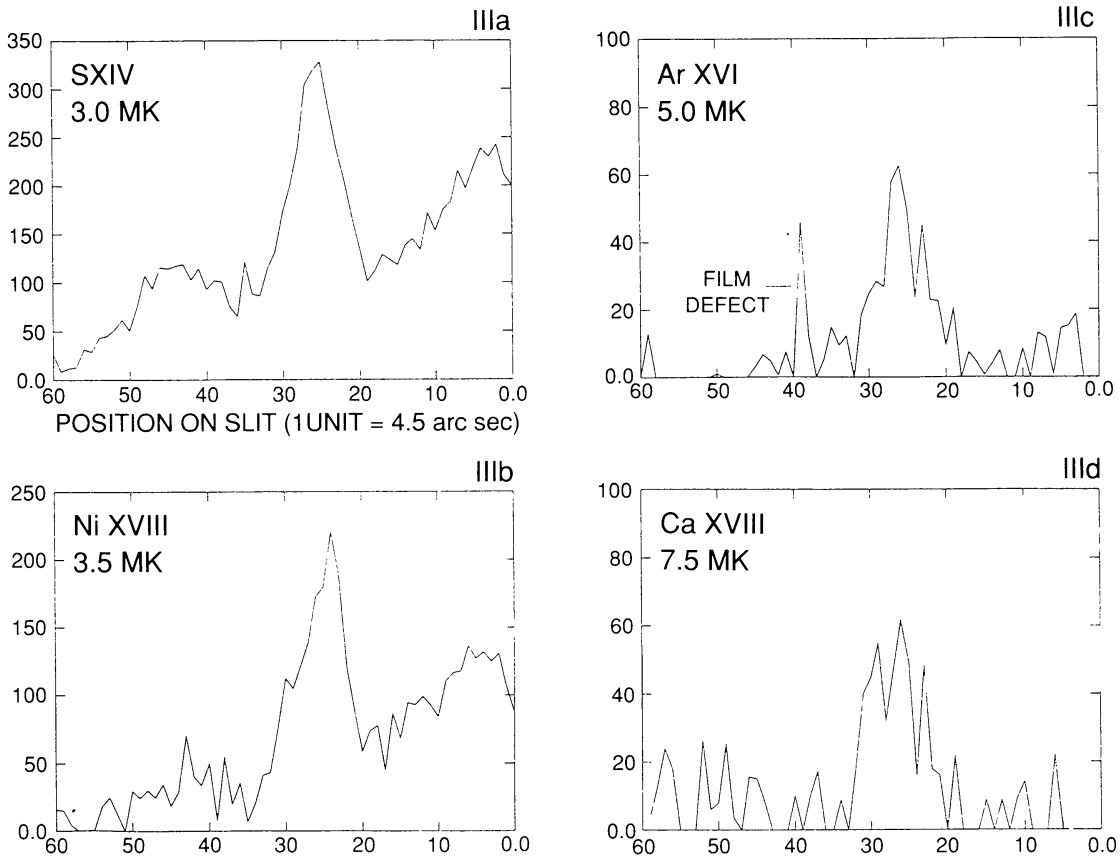

Fig. 9c.

Fig. 9. Distribution of radiation along the instrument slit and therefore along a line through the central portion of the active region in emission lines at temperatures from 40 000 K to 7.5 million K. The electron temperature for maximum relative population of the ion (Jordan, 1969; Landini and Monsignori Fossi, 1972) is given in each instance. (a) Transition region emission: He II, Ne VI, Mg VI, and Mg VIII. (b) Emission at coronal temperatures: Mg IX, Fe XIV, Fe XV, and Fe XVI. (c) Flare-enhanced high temperature emission: S XIV, Ni XVIII, Ar XVI, and Ca XVIII.

temperature gradient between the hot plasma represented by Ni XVIII and Ca XVIII emission and the underlying chromosphere must be very high, resulting in negligible emission measure for ions at intermediate temperatures.

5.3. Spectral emission line catalog

An emission line catalog has been derived from two sets of measurements made on a Grant microdensitometer (Thomas *et al.*, 1989). Integrating over the entire length of the slit images, 189 spectral features were noted on at least one run, of which 137 matched identified emission lines reported by Behring *et al.* (1976) or Kelly (1987) while 125 features were recorded on both runs, of which 107 matched reported lines. The observed emission lines cover the temperature range from 40 000 K (in He II) to 7.5 million K (in Ca XVIII) and offer a rich source of density diagnostics.

5.4 Observations of Doppler Shifts in EUV Emission Lines

Even a cursory visual examination of the SERTS spectra reveals that there are no appreciable shifts in the wavelengths (corresponding line-of-sight velocities of hundreds or even tens of km s^{-1}) on spatial scales resolved by the telescope. To determine the presence of lesser velocities requires careful measurement of the line positions in the direction of dispersion and analysis of probable errors introduced by the photographic granularity. Preliminary results indicate that RMS velocities derived from displacements of line centers are generally between 2 and 5 km s^{-1} prior to correcting for grain noise and between 0.8 (i.e., effectively zero) and 4.5 km s^{-1} after a correction has been applied. These net RMS Doppler velocities are significantly smaller than non-thermal velocities derived from excess line broadening that have frequently been reported with more spatially-averaged observations (Feldman and Behring, 1974; Cheng, Doschek, and Feldman, 1979). Such observations typically yield velocities of 10–30 km s^{-1} (and such velocities are still inferred from excess emission line widths present in our observations at spatial scales of 5–10 arc sec). We, therefore, can conclude that the excess broadening in prior observations cannot be due to averaging over differential mass motions on scales of 5000 km or greater. The only appreciable emission line shift observed with some certainty appeared in the emission line of Mg IX at 368.1 Å over a large sunspot and could be interpreted as an outward flow of 14 km s^{-1} relative to the mean position of the spectral line. Subsequent analysis (Brosius, 1991) has demonstrated that the coronal magnetic field (calculated in the potential approximation from observations of the longitudinal photospheric field) was aligned within 10° to the SERTS line of sight at the position at which the line shift was observed.

6. Summary

We have demonstrated the unique contribution that stigmatic imaging of the solar corona at EUV wavelengths can make in characterizing the state of the coronal plasma. Improvement of the SERTS instrument has continued, with the fabrication of a telescope with better optical surfaces and the application of multilayer coating technology to enhance the EUV reflectivity of the toroidal grating. Observations similar to those made by SERTS, but with higher spatial resolution, are planned by the Solar Ultraviolet Measurements of Emitted Radiation (SUMER) instrument on the Solar Heliospheric Observatory Mission (SOHO) at wavelengths between 500 and 1600 Å (Poland and Domingo, 1988). Such observations promise to reveal many new aspects of the dynamic solar atmosphere.

Acknowledgements

We would like to recognize the substantial contributions made by others during the course of this program. U. Feldman, a co-investigator on the original Shuttle/Spacelab proposal, has provided support and guidance over many years. Technical staff at the Goddard Space Flight Center, in particular C. Condor, J. Houston, C. Fleetwood,

M. Swartz, and J. Tebay have made major contributions in the design, execution, and calibration of the instrument. We also wish to recognize the support provided by R. Altrock and his staff of the Sacramento Peak Observatory of the National Solar Observatory, NOAO, by H. Jones of GSFC, at the Kitt Peak Observatory, National Solar Observatory, NOAO, and by the staff of the Space Environment Laboratory of NOAA in providing current information on solar activity during our field operations. We also are indebted to G. Brueckner of the Naval Research Laboratory for providing the EUV photographic film used on the SERTS flight. This research was supported under NASA RTOP 879–11–38.

References

Athay, R. G.: 1976, *The Solar Chromosphere and Corona: Quiet Sun*, D. Reidel Publ. Co., Dordrecht, Holland.
Billings, D. E.: 1966, *A Guide to the Solar Corona*, Academic Press, New York.
Behring, W. E., Cohen, L., Feldman, U., and Doschek, G. A.: 1976, *Astrophys. J.* **203**, 521.
Brosius, J. W.: 1991, private communication.
Burton, W. M., Hatter, A. T., and Ridgeley, A.: 1973, *Appl. Opt.* **12**, 1851.
Canfield, L. R., Johnston, R. P., and Madden, R. D.: 1973, *Appl. Opt.* **12**, 1611.
Cheng, C-C., Doschek, G. A., and Feldman, U.: 1979, *Astrophys. J.* **227**, 1037.
Cushman, G. W. and Rense, W. A.: 1978, *Solar Phys.* **58**, 299.
Feldman, U. and Behring, W. E.: 1974, *Astrophys. J.* **189**, L45.
Feldman, U., Doschek, G. A., and Widing, K. G.: 1978, *Astrophys. J.* **219**, 304.
Feldman, U., Doschek, G. A., Prinz, D. K., and Nagel, D. J.: 1976, *J. Appl. Phys.* **47**, 1341.
Haber, H.: 1950, *J. Opt. Soc. Am.* **40**, 153.
Haug, E.: 1979, *Astrophys. J.* **228**, 903.
Huber, M. C. E. and Tondello, G.: 1979, *Appl. Opt.* **18**, 3948.
Jordan, C.: 1969, *Monthly Notices Roy. Astron. Soc.* **142**, 501.
Kelly, R. L.: 1987, *J. Phys. Chem. Ref. Data* **16**, Suppl. 1.
Landini, M. and Monsignori Fossi, B. C.: 1972, *Astron. Astrophys. Suppl.* **7**, 291.
Mangus, J. D.: 1970, *Appl. Opt.* **9**, 1019.
Neupert, W. M. and Kastner, S. O.: 1983, *Astron. Astrophys.* **128**, 188.
Neupert, W. M., Chapman, R. D., Epstein, G. L., Feldman, U., Ionson, J. A., Michalitsianos, A., and Thomas, R. J.: 1978, *A Solar Extreme Ultraviolet Telescope and Spectrograph for Shuttle*, NASA Tech. Mem. 80643.
Neupert, W. M., Epstein, G. L., Thomas, R. J., and Feldman, U.: 1981, *Space Sci. Rev.* **29**, 425.
Osantowski, J. F.: 1974, *J. Opt. Soc. Am.* **64**, 834.
Poland, A. I. and Domingo, V.: 1988, *Adv. Space Res.* **8**(11), 101.
Rottman, G. J., Orrall, F. Q., and Klimchuk, J. A.: 1981, *Astrophys. J.* **247**, L135.
Samson, J. A. R.: 1967, *Techniques of Vacuum Ultraviolet Spectroscopy*, John Wiley and Sons, New York.
Thomas, R. J., Neupert, W. M., Cohen, L., and Thompson, W. T.: 1989, *Bull. Am. Astron. Soc.* **21**, 1149.
Thomas, R. J., Keski-Kuha, R. A. M., Neupert, W. M., Condor, C. E., and Gum, J. S.: 1991, *Appl. Opt.* **30**, 2245.
Tousey, R., Bartoe, J.-D. F., Brueckner, G. E., and Purcell, J. D.: 1977, *Appl. Opt.* **16**, 870.